KANSAS GEOLOGICAL SURVEY
OPEN-FILE REPORT 1995-57

A High-frequency Ground-penetrating Radar Study
of the Captain Creek Limestone,
Johnson County, Kansas

by

Alex Martinez
Joseph M. Kruger
Evan K. Franseen
Mike L. Shoemaker
Michael S. Roark

Disclaimer

The Kansas Geological Survey does not guarantee this document to be free from errors or inaccuracies and disclaims any responsibility or liability for interpretations based on data used in the production of this document or decisions based thereon. This report is intended to make results of research available at the earliest possible date, but is not intended to constitute final or formal publications.

Kansas Geological Survey
1930 Constant Avenue
University of Kansas
Lawrence, KS 66047-3726

A High-Frequency Ground-Penetrating Radar Study of The Captain Creek Limestone, Johnson County, Kansas

Kansas Geological Survey Open File Report 95-57

Alex Martinez[1], Joseph M. Kruger[1], Evan K. Franseen[1],
Mike L. Shoemaker[2], Michael S. Roark[2],

[1]Kansas Geological Survey, Lawrence, KS
[2]University of Missouri-Rolla, Rolla, MO

INTRODUCTION

A pilot study to determine the usefulness of high-frequency ground-penetrating radar (GPR) methods in delineating geometries, erosional truncation surfaces, and internal bedding features within carbonate strata near the surface was undertaken in the Spring of 1995. High-frequency ground-penetrating radar methods are capable of resolving shallow subsurface features in great detail in a manner analogous to reflection seismic data. This has the potential of allowing internal geometries and bedding features of near surface rock units to be studied beyond outcrop faces and adding stratigraphic information to databases where outcrop information is limited.

This report focuses on an outcrop in northwest Johnson, County, Kansas (SQE-1 of Cunningham and Franseen, 1992) (Fig. 1). Two 106 m (350 ft) long profiles of GPR data were gathered at this study site aimed at imaging features associated with the Captain Creek Limestone Member of the Stanton Limestone (within the Stanton depositional sequence of Watney et al., 1989) and the underlying Vilas Shale, which caps the subjacent Plattsburg depositional sequence of Watney et al. (1989). The study site was chosen in order to determine the capabilities of GPR to image: 1) the erosional contact between the Captain Creek Limestone and Vilas Shale; 2) the contact between the lower and upper Captain Creek Limestone submembers; and 3) internal bedding geometries and truncations, including foreset beds, in the lower and upper Captain Creek submembers.

GEOLOGIC SETTING

The Vilas Shale is typically a gray mudstone, silty or sandy shale, or fine-grained sandstone containing common mica and carbonized plant fragments (Cunningham and Franseen, 1992). The Vilas Shale represents deltaic sedimentation during a relative low stand in base level and the upper surface is considered the sequence boundary of the Plattsburg depositional sequence (Watney et al., 1989).

The Captain Creek Limestone is the flooding unit within the Stanton depositional sequence and represents initial carbonate sedimentation during a relative rise in sea level (Watney et al., 1989). Cunningham and Franseen (1992) proposed two submembers for the Captain Creek Limestone. The lower submember is composed of a gray or brown conglomeratic lime grainstone composed of small pebble-sized limestone clasts, bioclasts, and shale clasts and locally containing 1-3 dm-scale horizontal bedding and local foresets (Cunningham and Franseen, 1992). The upper Captain Creek submember is more massively bedded and typically occurs as a gray to light-brown phylloid, brachiopod, crinoid and bryozoan lime wackestone-packstone (Cunningham and

Franseen, 1992). At the study site (SQE-1 of Cunningham and Franseen, 1992), the two submembers are separated by a 0.25 m-thick slightly fissiliferous to blocky sandy shale.

Cunningham and Franseen (1992) noted thickening and thinning trends of the lower Captain Creek conglomerate submember that were related, at least in part, to paleobathymetry produced by phylloid algal buildups within the Argentine and Farley Limestone Members of the Wyandotte Formation and the Plattsburg Limestone. The contact of the lower Captain Creek conglomeratic submember with the Vilas Shale indicates some erosional modification and is interpreted as a sequence boundary resulting from a relative sea-level fall. Cunningham and Franseen (1992) interpreted the Captain Creek conglomerates to have been deposited as tidal channel fills in bathymetrically constricted areas between the Bonner Springs and Olathe algal mounds during a relative sea-level rise.

GPR METHODS, DATA COLLECTION, AND PROCESSING

Methods

Ground-penetrating radar (GPR) is a high-resolution near-surface geophysical technique using antennas to send electromagnetic pulses into the ground in order to image the subsurface via returned reflection energy. Similar to seismic reflection methods, where reflections are caused by boundaries associated with acoustical impedance contrasts, GPR reflections are caused by the electromagnetic waves encountering media of different electrical properties - namely boundaries consisting of a contrast in the dielectric constant of the material above and below the boundary. Values for dielectric constants (K) range from 1 for air, 3-5 for dry sand, 4-8 for limestone, 5-13 for shale, 5-40 for clay, and 81 for water (Davis and Annan, 1989). Dielectric constant values affect the velocity of electromagnetic waves through a material, and are related to velocity in non-magnetic materials by:

$$\text{velocity} = \frac{c}{\sqrt{K}}$$

where $c = 3 \times 10^8$ m/s (speed of light in a vacuum). Using the relationship given above, one-way velocities for materials range from 0.3 m/ns (meters/nanosecond) for air, 0.134-0.173 m/ns for dry sand, 0.11-0.15 m/ns for limestone, 0.077-0.134 m/ns for shale, 0.047-0.134 m/ns for clay, and 0.033 m/ns for water. Antenna frequencies typically range from 10 MHz to 1000 MHz (a 500 MHz antenna was used in this study), and imaging resolution is proportional to antenna frequency, while penetration depth is inversely proportional to antenna frequency (the greater the antenna frequency, the less penetration but greater detail). Vertical resolution varies from 1-1.5 m (3-5 ft)

for low-frequency antennas (10-100 MHz), to 0.02-0.3 m (1-12 in) for high-frequency antennas (500-1000 MHz) for most materials (Davis and Annan, 1989).

GPR profiles have a similar appearance to seismic profiles, and usually are represented as common depth point (cdp) data, with amplitude variations representing differences in reflection energy. As with seismic data, vertical scales are in time (or depth if the data have been depth migrated), while lateral scales are in distance. However, the scales differ by several orders of magnitude; GPR records have lengths measured in nanoseconds ($1x10^{-9}$ s), compared to milliseconds ($1x10^{-3}$ s) in seismic records. Also, the distances between cdps in GPR profiles are usually much smaller than seismic profiles (an average GPR cdp spacing of 3 cm in this study, versus standard, near-surface seismic reflection cdp spacing of 0.3-1.5 m for high-resolution profiles).

Equipment & Data Collection

Preparation of the study site included clearing the antenna path of obstructions, flagging stations along the antenna path, collecting relative elevation information for the stations, and obtaining photomosaics of the outcrops in relation to the stations. The clearing of material such as small rocks and clumps of grass from the antenna pathway greatly enhanced the coupling of the antenna with the ground during the data collection process. In addition, by clearing the pathway of obstructions, lateral movement of the antenna stayed at a relatively consistent velocity and ensured even cdp coverage. Station flagging at a 1.5 m (5 ft) interval served several purposes. It assisted in retaining the same antenna pathway for each of the various scan lengths (record lengths). It also allowed the GPR data to be correlated to specific ground locations via photomosaics, and ensured some lateral control during data collection. The collection of relative elevation information from stations every 7.6 m (25 ft) allowed the data to be corrected for elevation differences during processing. These corrections immensely aided the interpretation of reflection information and correlation with outcrop information. Elevations were obtained using a level and rod, and are accurate to within $\pm$ 3 cm. The photomosaics were gathered in increments of 7.6 m (25 ft) and allow correlation between the outcrop and GPR data.

The equipment used for the study was a GSSI SIR System-8 GPR unit, with a DT6000A tape unit and 500-MHz dominant-frequency monostatic antenna (transmitting and receiving antenna the same). Use of a monostatic system allowed for rapid acquisition but precluded measurement of any velocity information. Because of this, depth conversions were not performed. Scan lengths of 60 and 80 ns were recorded at a rate of 12.8 scans/second as the antenna was pulled along the line. Only the 80 ns data is presented in this report because it imaged deeper strata than the 60 ns scan. The tape unit recorded coherent system noise beginning at approximately 40 ns on each

trace. This noise masked most of the reflection information below 40 ns, greatly reducing the signal-to-noise ratio at the longer scan times. Digital filtering of the data removed some, but not all, of the noise. A short marker-pulse was recorded whenever passing a flagged station (every 1.5 m; 5 ft), and a double pulse was recorded at every fifth flag (every 7.6 m; 25 ft). This enhanced control over how fast the antenna was pulled along the ground, and allowed correlation between the data and the outcrop.

Data Processing

The data were downloaded from the DT6000A tape unit and converted from RADAN format into 4-byte SEGY format before importation into Seismic Unix (SU) on a workstation. Once within SU, the data were time- and distance-scaled by a factor of $1x10^6$ for viewing and processing purposes. The 80 ns scan data had 512 samples per trace, a sample interval of 0.156 ns, and a lateral distance (cdp trace spacing) of approximately 3 cm per trace.

The GPR data were treated as stacked seismic reflection data within SU, opening up the possibility of post-stack digital processing. The basic data processing flow is shown in Figure 2. Front-end mutes removed high-amplitude first arrivals, allowing trace balancing to enhance low-amplitude reflection information recorded later in the data. Coherent noise filtering removed most of the lateral system noise recorded in the regions below 40 ns in the data. Bandpass and frequency-wavenumber (f-k) filters reduced the lower frequency information and enhanced high-frequency reflections. Trace balancing via automatic gain controls (AGC) allowed some of the low-amplitude events to become more visible. The data were then elevation corrected to an arbitrary datum at the highest elevation along the line to remove the longer period elevation static shifts that inhibit correlation with the outcrop, and prevent the loss of any data. Therefore, the top of the data on the GPR sections roughly corresponds to the surface.

RESULTS

General Results

A site map of the study area shows the relationship between the GPR line and the outcrop (Fig. 3). Station locations on the photomosaics (Figs. 4a-6a) are indicated by survey crew members holding station number signs while standing on the stations. The stations are indicated on the GPR data by vertical pulse lines on the sections every 1.5 m (5 ft) and double lines every 7.6 m (25 ft). The data are plotted down to approximately 70 ns below the surface. This

corresponds to a depth of 4.3 m (14 ft) assuming an average one-way velocity of 0.12 m/ns (0.4 ft/ns), which is appropriate for limestone (Davis and Annan, 1989). The best data from the GPR profile occurs east of station 50, and west of station 150 where the soil cover is relatively thin (Figs. 4-6). Between these stations, the data are mostly noise and are not included in this report. Uninterpreted copies of the GPR data and outcrop mosaics shown in Figures 5 and 6 are given in Appendix A.

In the western part of the line, relatively high amplitude coherent reflections (Figs. 5b and 6b) are correlated with major stratigraphic divisions visible on the outcrop and are indicated by the heavy dashed lines (Figs. 5a and 6a). These divisions are the top of the upper Captain Creek Limestone (UC1), the top of the lower Captain Creek Limestone submember (LC1), and the top of the Vilas Shale (VS1). In addition, reflections between the major unit divisions are also identified by thin dashed lines and correlated as close as possible with bed boundaries or other features visible on the outcrop. Although an exact correlation between a given reflection and a given bedding surface may not be possible in all cases due to a lack of precise depth control on the GPR sections, overall the geometries indicated by the GPR interpretation correlate quite well with the outcrop data. Correlations between true reflections and the outcrop are also complicated by instrument generated noise which creates events that are parallel to the top of the GPR data (elevation corrected surface) and extend downward throughout the data. Because of the AGC applied during processing, this noise is particularly apparent where the true reflective signal is weak or nonexistent. It is generally easy to ignore the noise when it cuts across the true reflections, but it may complicate interpretation where it is parallel or subparallel to the reflective fabric. A barbed wire fence which parallels the GPR line just south of it does not appear to have any affect on the data. Likewise, the trees behind the fence and the outcrop-air interface do not appear to adversely affect the data either.

Soil Layer

The top of the road cut where the GPR profiles were gathered has a rough, rocky terrain on either end, and a thick overburden in the middle. The overburden thickness ranges from 0-1 m, consists of a fine, silty soil with approximately 45% clay, 40% silt, 15% sand, and contains small fragments of chert and limestone. The clay-rich soil cover caused massive signal attenuation with the high-frequency antenna, resulting in no discernible reflection energy between stations 50 and 150 where the soil is relatively thick. The thickening soil also causes a velocity pull-down of reflections between stations 40 and 190 due to the change in velocity between the slower clay-rich overburden and the faster limestone (Figs. 4 and 5). Minor variations in soil thickness and velocity, as well as minor changes in topography that occur between elevation measurements, also

result in some of the short period static shifts or waviness exhibited by the GPR data. Some of this pattern, however, may also be due to intersecting hyperbolic diffractions caused by open or soil filled fractures near the surface, or irregularities in bedding surfaces within the limestone.

Upper Captain Creek Limestone

The top of the upper Captain Creek Limestone submember (UC1) is indicated by a prominent reflection imaged between station 155 and station 200 where the reflector reaches the surface (Fig. 5). Material above this reflector is primarily soil which, from the high clay content, may have been created from an overlying shale. Thus, this boundary may be the contact between the Captain Creek Limestone and Eudora Shale. This reflector is also imaged between stations 35 and 55 (Fig. 4).

Soil filled fractures near the top of the limestone may cause the interruption of continuity seen in the reflection near stations 185 and 190, and result in weak diffractions (convex upward hyperbolic events) near the contact at these stations. Another more prominent diffraction near the surface in the upper Captain Creek Limestone, which is likely caused by a soil filled fracture, occurs between stations 210 and 215. Other evidence for fracturing includes a velocity pull-down of reflections at station 190, and dipping events in the lower half of the submember between stations 195 and 210 adjacent to an isolated less disturbed block between stations 200 and 205 (thinner dashed lines in Fig. 5).

Several horizontal to low-angle dipping limestone layers in the upper Captain Creek Limestone submember are clearly visible and traceable laterally until they intersect the modern-day surface between stations 190 and 250 (Figs. 5a and 6a). Reflections from these beds are also visible on the GPR data. Some of these are marked by thinner dashed lines and indicate a gradual thinning of beds to the west (Figs. 5b and 6b).

Lower Captain Creek Limestone

The contact between the lower and upper Captain Creek Limestone submembers, marked by a 0.25 m-thick sandy shale, is clearly visible and traceable between stations 180 and 275 as reflector LC1 (Figs. 5 and 6). The fact that this relatively thin bed of sandy shale is sandwiched between limestone may add to the higher amplitude nature of the reflection due to constructive interference between reflections from the top and base of the shale. However, the double cycle nature of this reflector (two larger amplitude parallel reflections) may indicate that both the top and base of the shale are imaged in some areas (e.g. stations 235-245). It is also possible that the lower reflection is actually a prominent sidelobe related to the shape and duration of the radar pulse

and not to the strata.

Internal bedding geometries within the lower Captain Creek Limestone are also imaged by the GPR (Fig. 6b). Local convergent and divergent bedding geometries within the lower Captain Creek Limestone submember are especially visible between stations 240 and 285. These features and some truncations of beds at the base of the upper Captain Creek Limestone (between stations 225 and 250) are likely associated with crossbedding, which is common within the lower Captain Creek Limestone. The best crossbed foresets, clearly visible on outcrop east of station 225, are not imaged by GPR due to rapid signal attenuation caused by the relatively thick soil overburden in those areas. However, crossbed foresets are imaged on the GPR data in the lower half of the lower Captain Creek Limestone between stations 240 and 255. These crossbeds appear to terminate against a relatively flat lying bed above in both the outcrop and GPR data (Fig. 6). Bed thinning is apparent on the outcrop west of station 270. It is also visible on the GPR data as a decrease in time between more prominent reflections, and in some cases, termination of reflections.

Loss of reflection coherency, velocity pull-ups and velocity pull-downs occur between stations 270 and 285 in the lower Captain Creek Limestone (Fig. 6a). These features are probably due to variations in soil thickness and velocity, along with the surface exposure of beds with varying velocity along the profile (e.g. outcrop of the sandy shale at the contact between the upper and lower Captain Creek Limestone). Some of these features may also be due to fracturing of the limestone or minor structural disruption due to the weathering process. Some of the pull-up west of station 265 does appear to be geological though, as indicated by the upward bending of beds on the outcrop (Fig. 6).

Vilas Shale

The contact of the Captain Creek and Vilas Shale is clearly visible and traceable between stations 235 and 300 as reflector VS1 (Figs. 5 and 6). The strength of this reflection is probably due to the large contrast in dielectric constants between the limestone and shale. Because of signal attenuation caused by increasing soil thickness, this contact is not imaged by the GPR east of station 240. Truncation of some beds within the Vilas Shale that are visible on the outcrop are not clearly imaged on the GPR line. Sparse reflectivity within the Vilas Shale is probably due to the attenuating nature of most shales on the GPR signal.

As with the lower Captain Creek Limestone beds above it, the Vilas Shale appears to be slightly upwarped west of station 265 (Fig. 6). However, the reflection associated with the top of the shale is subject to the same velocity affects as the limestone above it, which may add to some of the apparent warping on the GPR data. Some evidence for true structural disruption of the shale comes from a diffraction which appears to emanate from the contact between the Vilas Shale and

overlying lower Captain Creek Limestone near station 270 (Fig 6b). This diffraction may be due to a fracture or small fault that appears to be responsible for the northward offset in the outcrop face near this station (Fig. 6a).

CONCLUSIONS

High-frequency GPR is clearly able to image boundaries between limestone and shale units in the shallow subsurface. Large amplitude reflections are also visible between limestone submembers when a relatively thin shaley bed separates them. This suggests that GPR may be used as a tool to extend such boundaries beyond the outcrop, and map them in the shallow subsurface.

The GPR technique images features such as truncated and disrupted beds, and isolated blocks that were formed due to modern erosion, weathering, and fracturing. The capability of GPR to image these features has important implications for imaging similar features that could be associated with ancient paleosol and karst development.

Internal bedding geometries within the limestone submembers are also imaged by GPR. These include crossbeds, convergent and divergent bedding, and truncation of beds. This indicates that high-resolution GPR can be used for imaging relatively small scale limestone bedding structures close to the surface.

Successful application of high-frequency GPR (using a 500 MHz antennae) depends on the absence of a relatively thick soil cover in areas where the soil has a high concentration of conductive clays. A relatively thick shale unit will also cause rapid signal attenuation and lack of penetration. Thus, when soil conditions and rock types are appropriate for the use of this technique, high-resolution GPR can aid in the detailed study of limestone units down to depths of 3-4 m or more.

ACKNOWLEDGMENTS

We would like to thank Dr. Neil Anderson from the University of Missouri-Rolla, for the use of UMR's GPR equipment and his assistance during data collection. We would also like to thank Scott Beaty for his assistance in the gathering of soil samples from the study site, Rich Sleezer for performing the soil analysis, and Tim Carr for making Kansas Geological Survey funds available for the survey.

REFERENCES

Cunningham, K.J. and Franseen, E.K., 1992, Conglomeratic Limestones of the Upper Pennsylvanian Captain Creek Limestone and Their Association with the Lower Sequence Boundary of the Stanton Depositional Sequence, Northwestern Johnson County, Kansas: Kansas Geological Survey Open-File Report 92-51, 47 p.

Davis, J. L. and Annan, A. P., 1989, Ground-Penetrating Radar for High-Resolution Mapping of Soil and Rock Stratigraphy: Geophysical Prospecting, v. 37, p. 531-551.

Watney, W.L., French, J.A., and Franseen, E.K., eds., 1989, Sequence Stratigraphic Interpretations and Modeling of Cyclothems in the Upper Pennsylvanian (Missourian), Lansing and Kansas City Groups in Eastern Kansas: Kansas Geological Society Guidebook, 41st Annual Field Trip, October 14-15, 1989, Kansas Geological Survey Open-File Report 89-44, 211 p.

Figure 1. Map showing the location of the Captain Creek Limestone ground-penetrating radar study site in eastern Kansas.

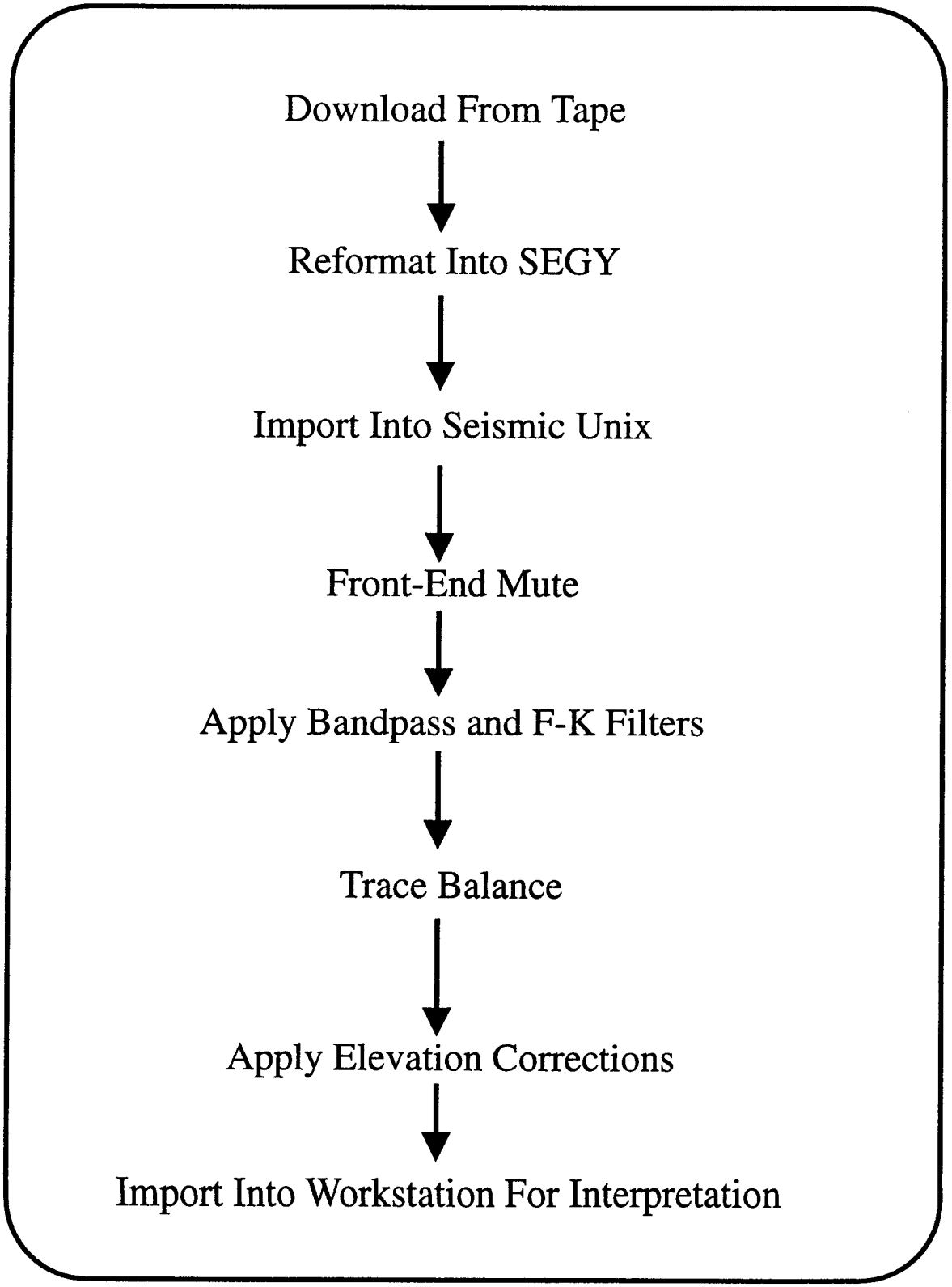

Figure 2. A generalized ground-penetrating radar data processing flow chart. Note that the steps taken are very similar to conventional post-stack seismic data processing.

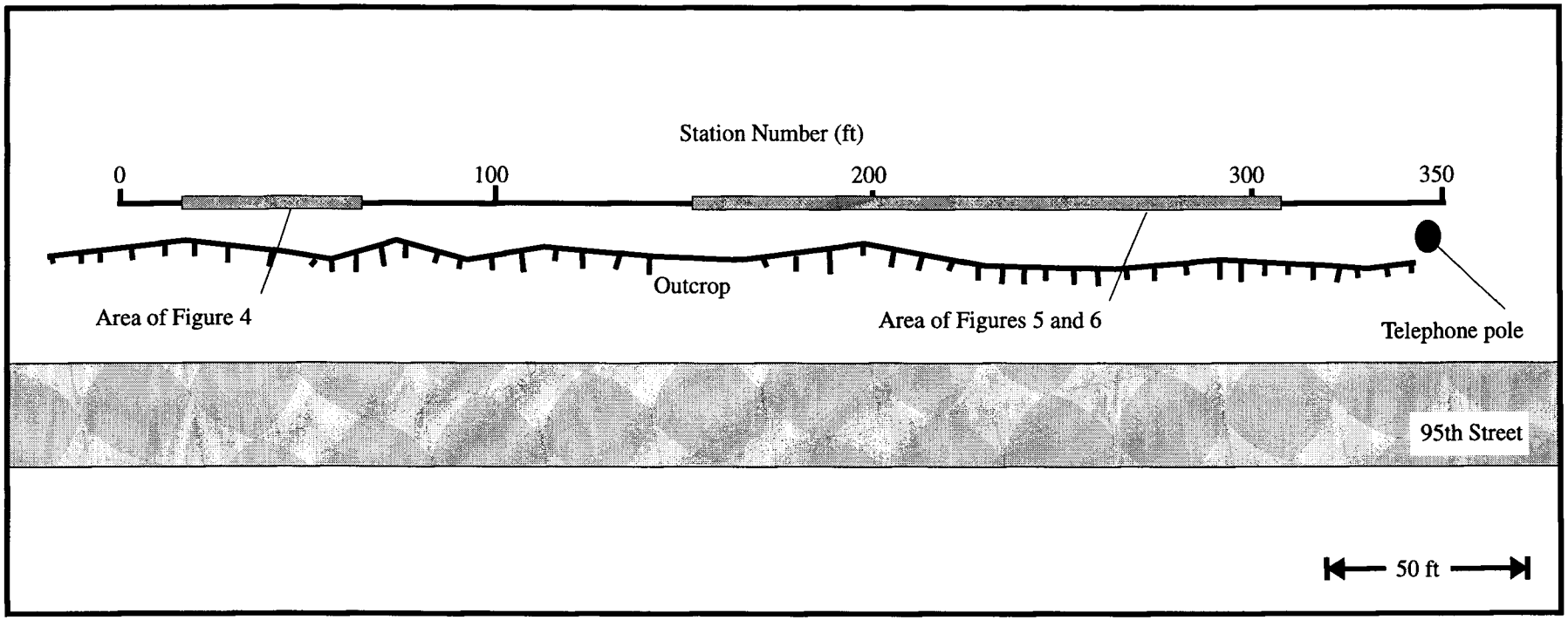

Figure 3. Map of study site detailing the extent of the outcrop, the GPR profile location, and the profile regions shown in Figures 4-6.

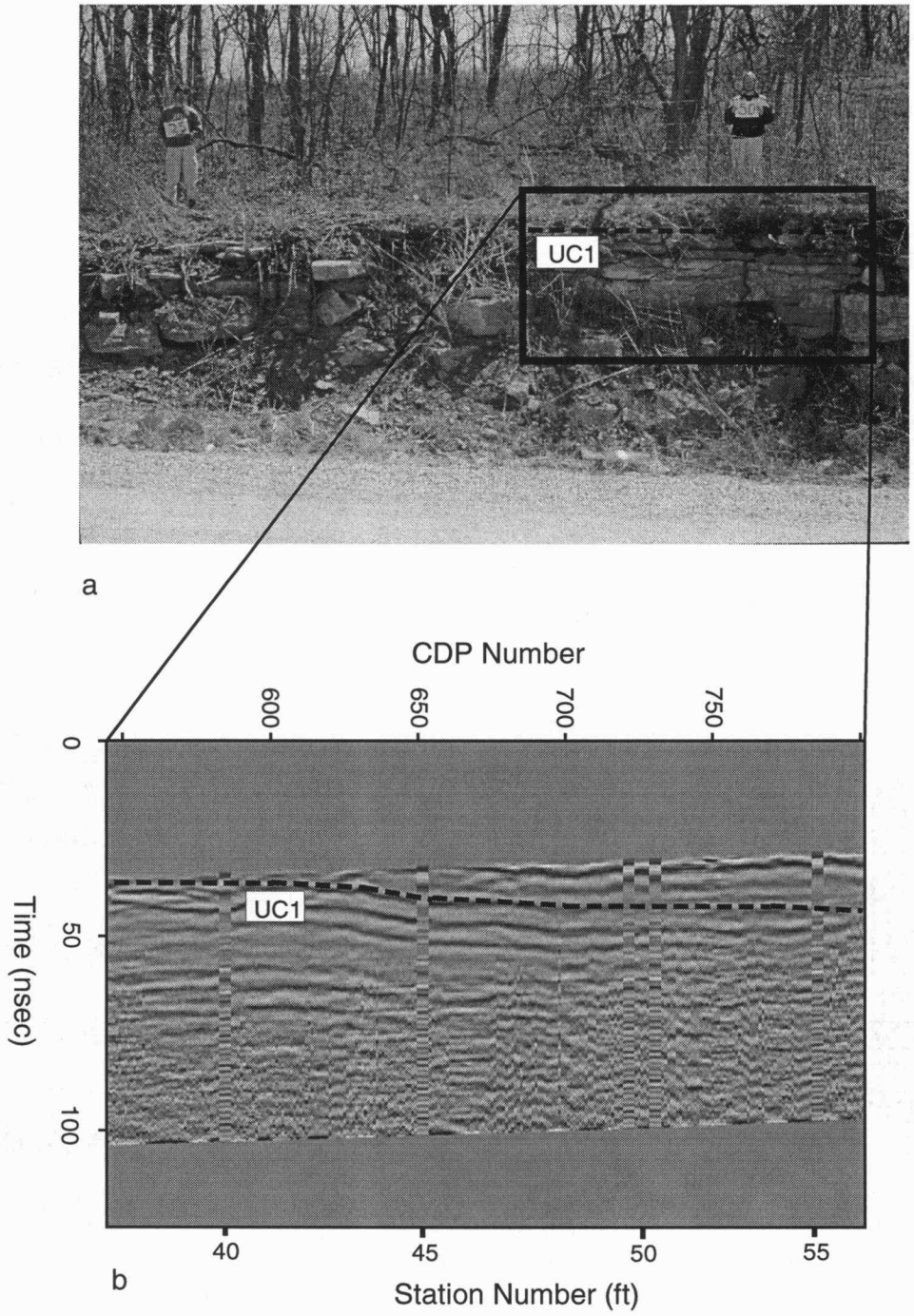

Figure 4. The effects of the low-velocity overburden on the GPR profile are seen in this display. The soil/bedrock interface (UC1, which has been interpreted as the top of the Upper Captain Creek Limestone) is shown as a dashed line on both the photomosaic and the GPR profile. The clay-rich soil causes GPR reflection information from the soil/bedrock interface to be time-delayed and attenuated.

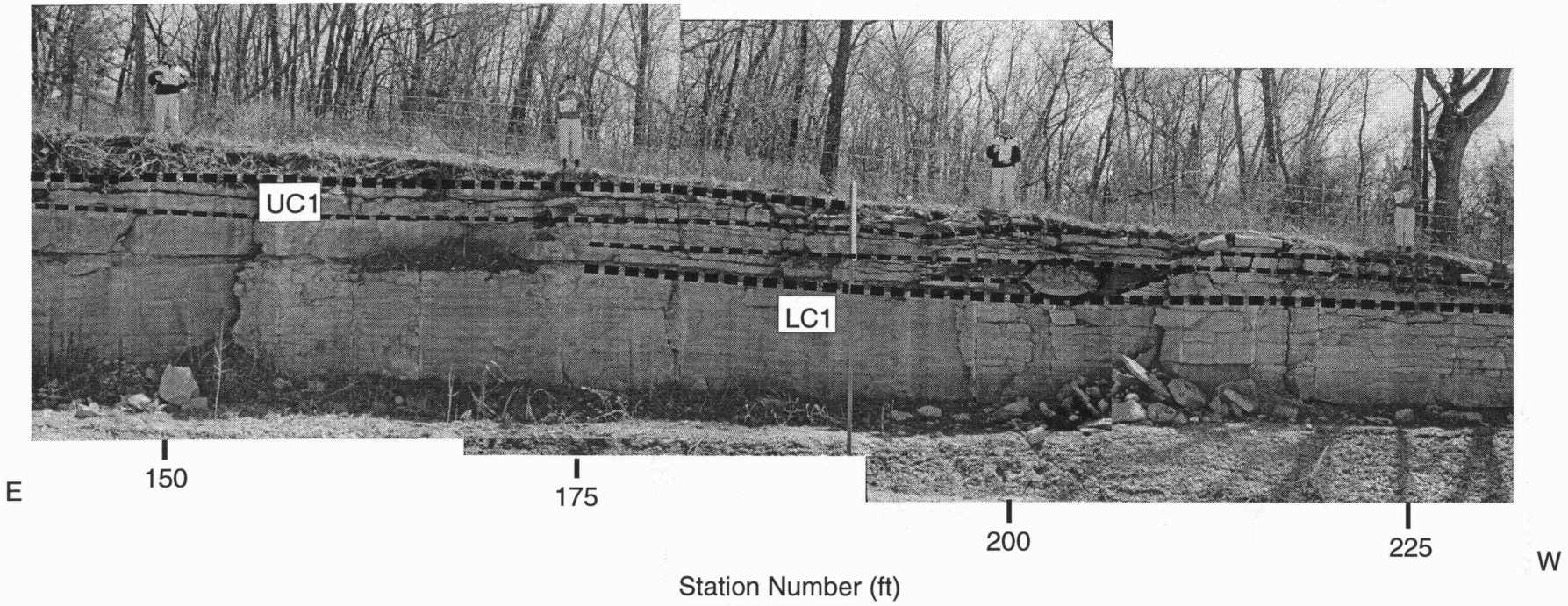

Figure 5a. Interpreted photomosaic of the western portion of the outcrop. The stations shown here (150-225) correspond to those shown in Figure 5b.

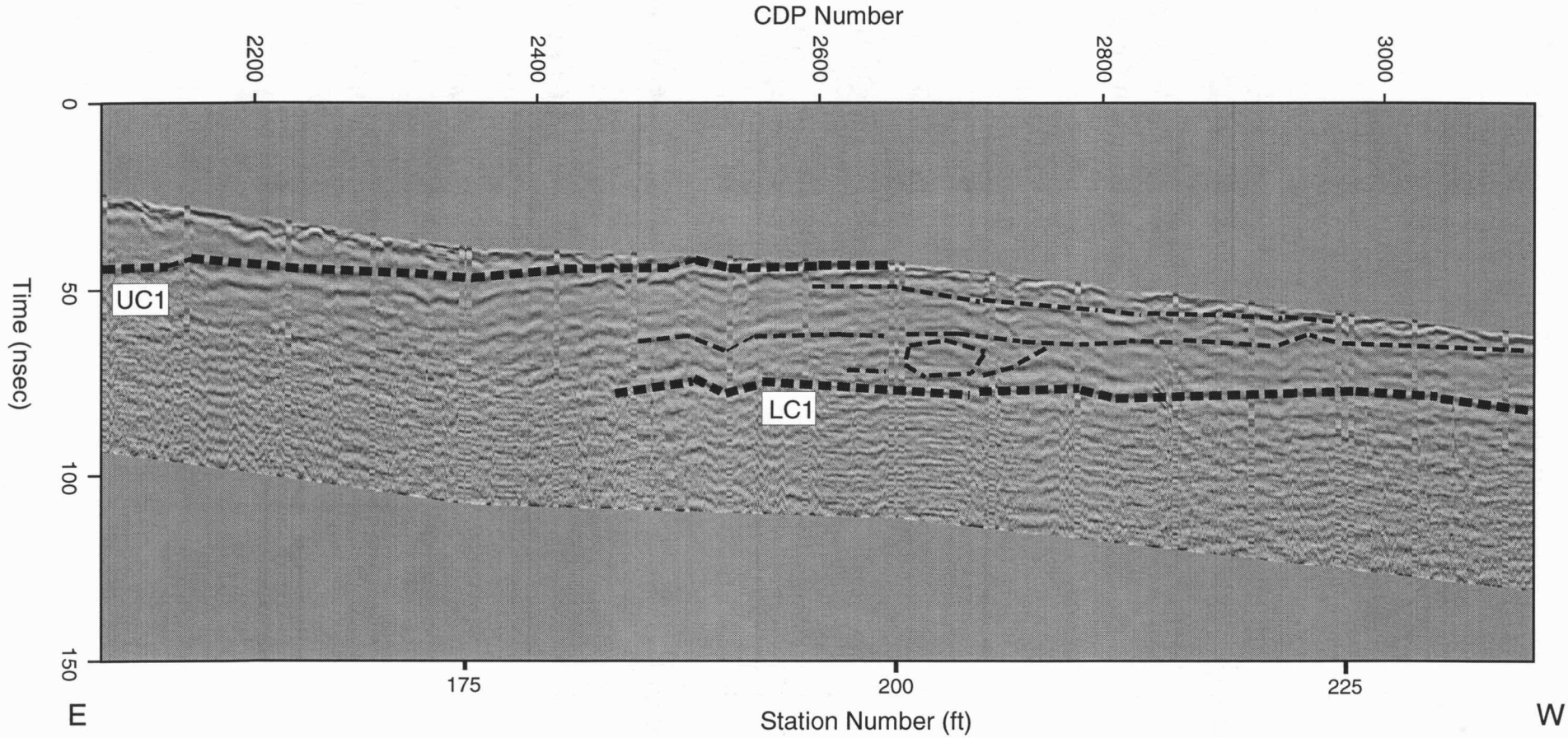

Figure 5b. The western portion of the GPR profile is shown here. The interface between the overburden and the top of the Upper Captain Creek Limestone is shown as horizon UC1. The contact between the Upper and Lower Captain Creek Limestones (horizon LC1) is also visible, as are internal features (some from modern weathering) within the Upper Captain Creek Limestone. The westward continuation of the GPR profile is shown in Figure 6b

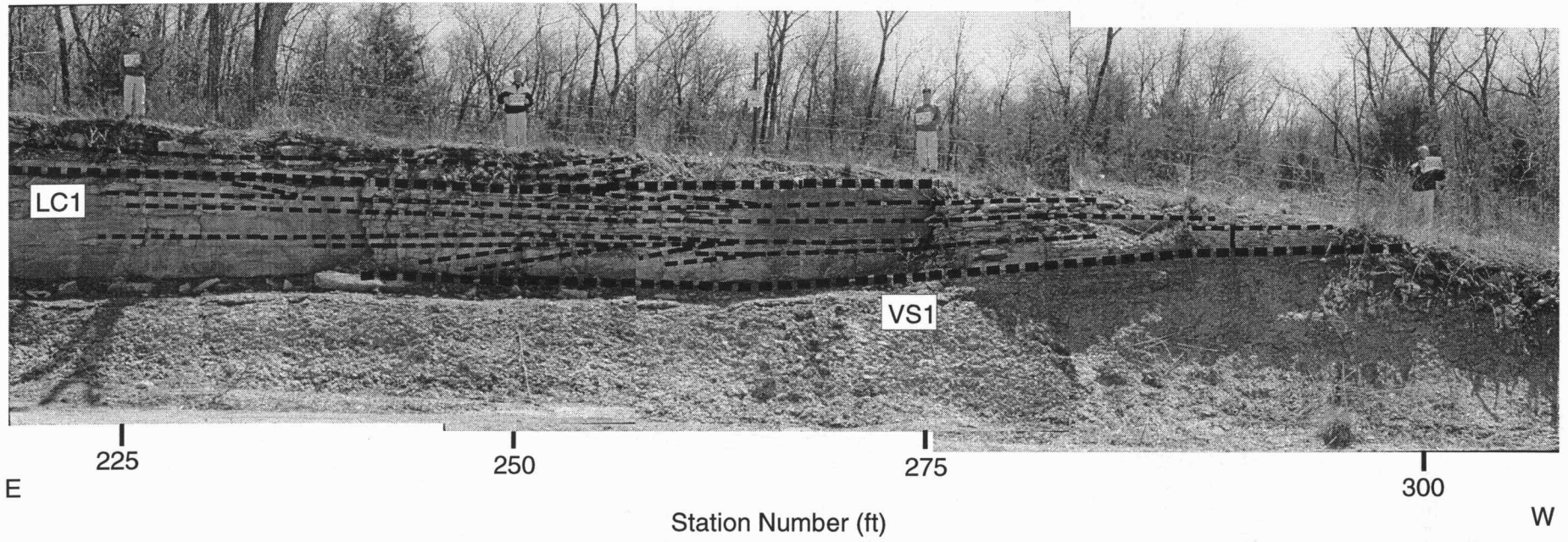

Figure 6a. Interpreted photomosaic of the western portion of the outcrop. The stations shown here (225-300) correspond to those shown in Figure 6b.

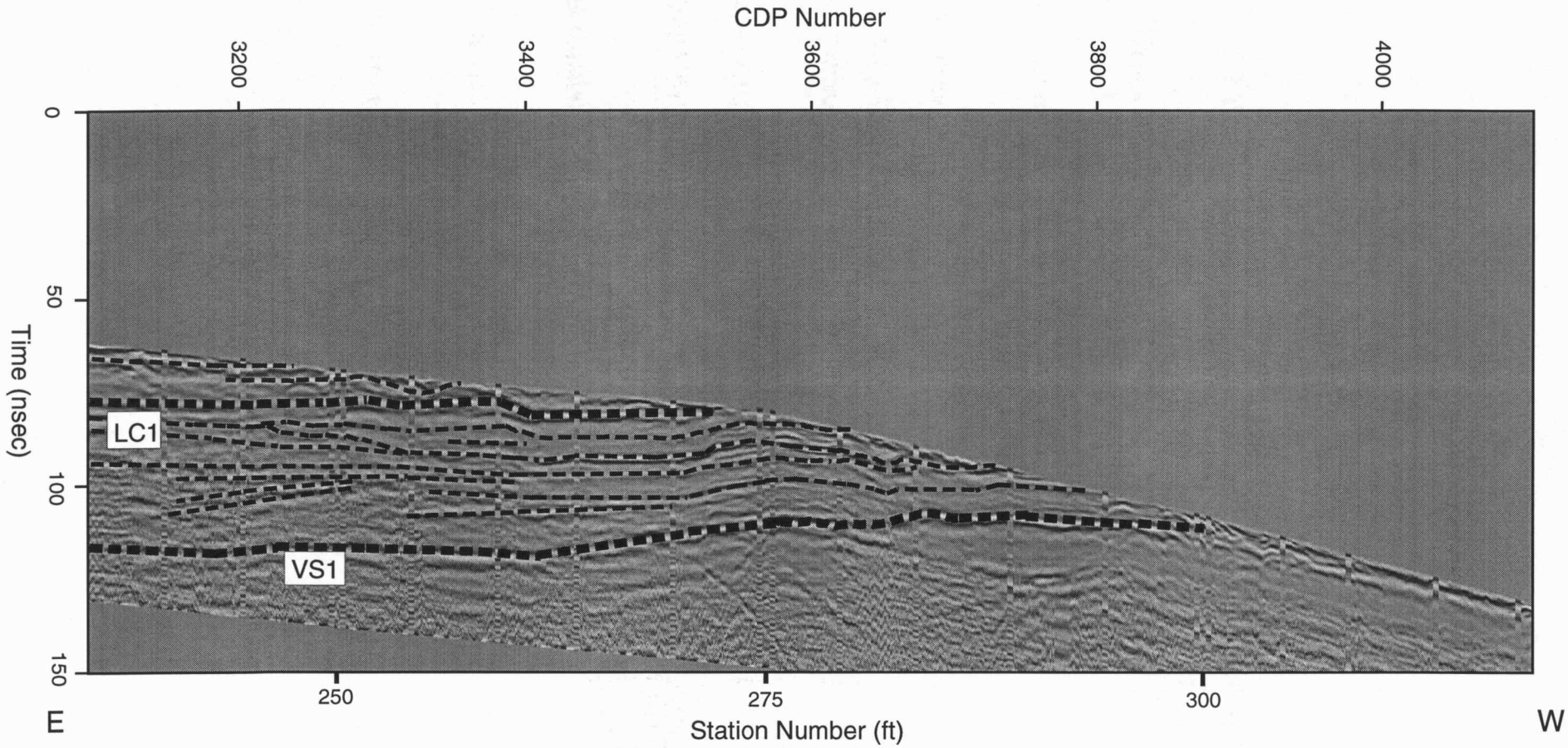

Figure 6b. The western portion of the GPR profile. Horizon VS1 is the contact between the top of the Vilas Shale and the bottom of the Captain Creek Limestone; and horizon LC1 is the top of the Lower Captain Creek Limestone. Numerous small-scale horizontal features are visible within the Lower Captain Creek Limestone on this display. The region within the shale (VS1) is relatively uniform in nature and does not contain many visible reflection features. The eastern continuation of the GPR profile is shown in Figure 5b.

APPENDIX A: UNINTERPRETED DATA

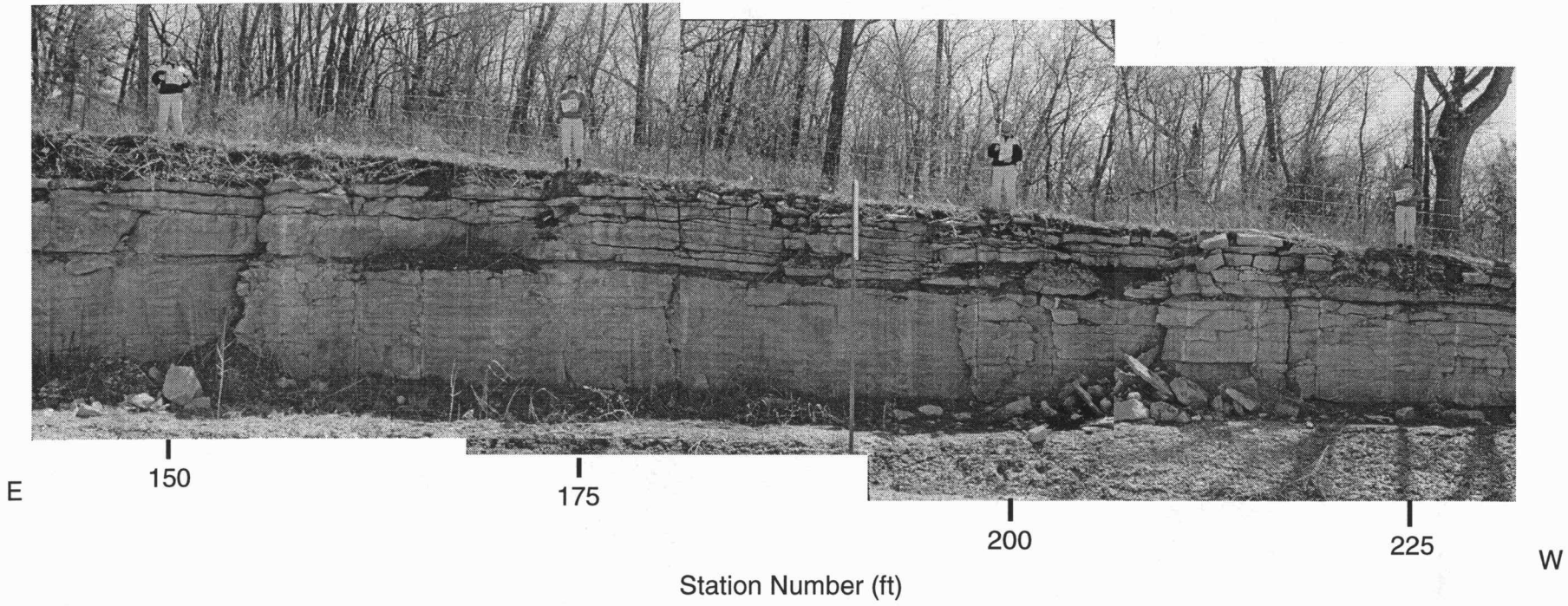

Figure 5a. Uninterpreted photomosaic of the western portion of the outcrop. The stations shown here (150-225) correspond to those shown in Figure 5b.

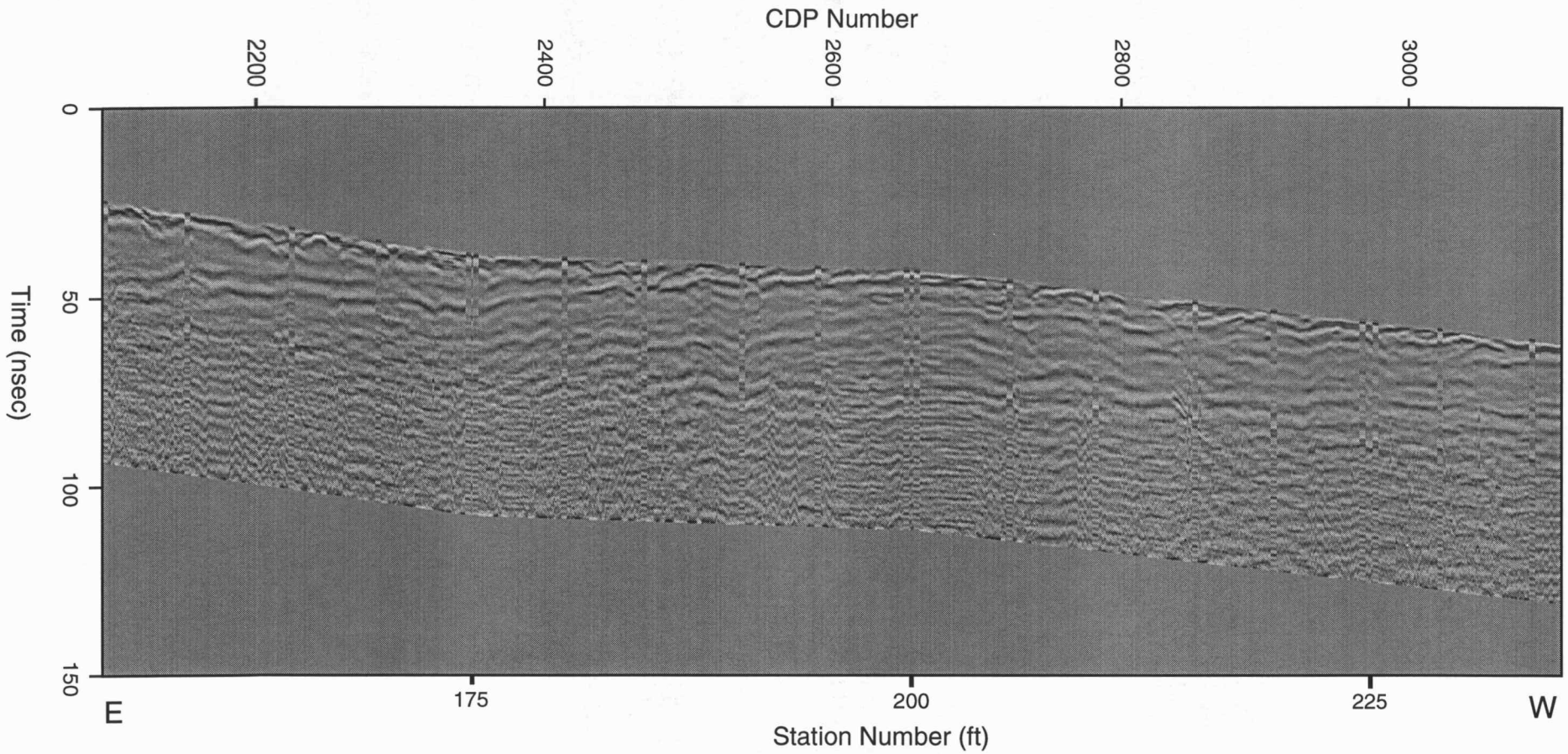

Figure 5b (Uninterpreted). The western portion of the GPR profile.

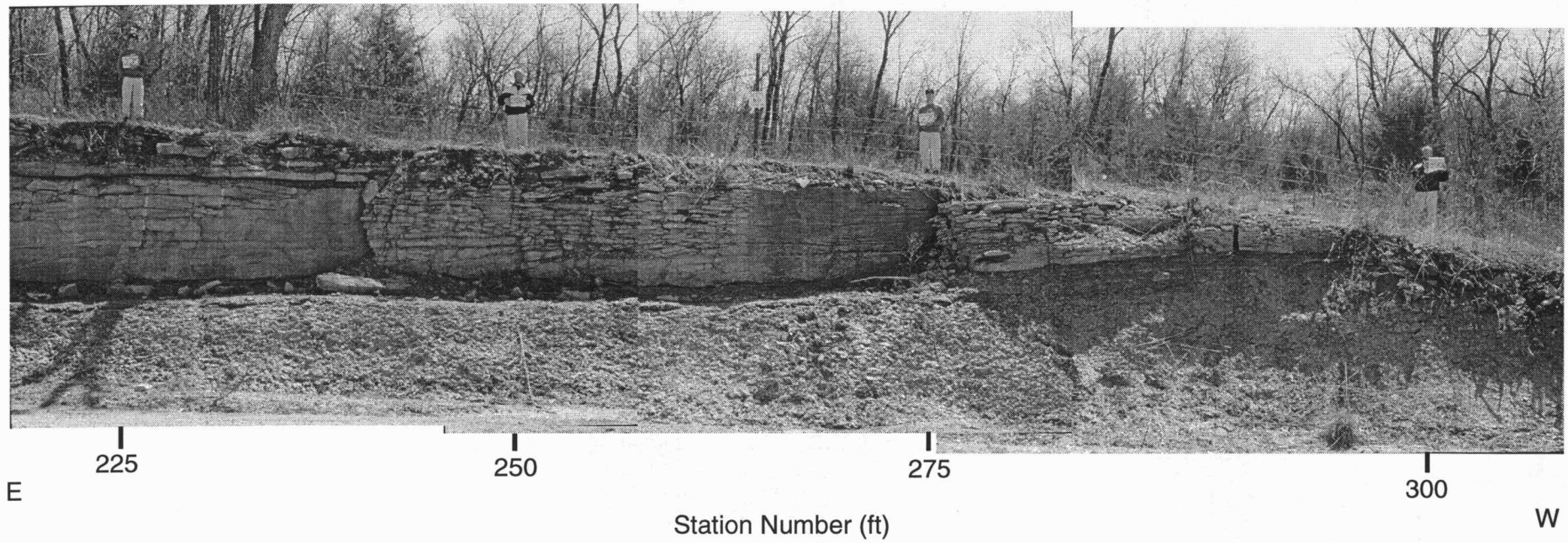

Figure 6a. Uninterpreted photomosaic of the western portion of the outcrop. The stations shown here (225-300) correspond to those shown in Figure 6b.

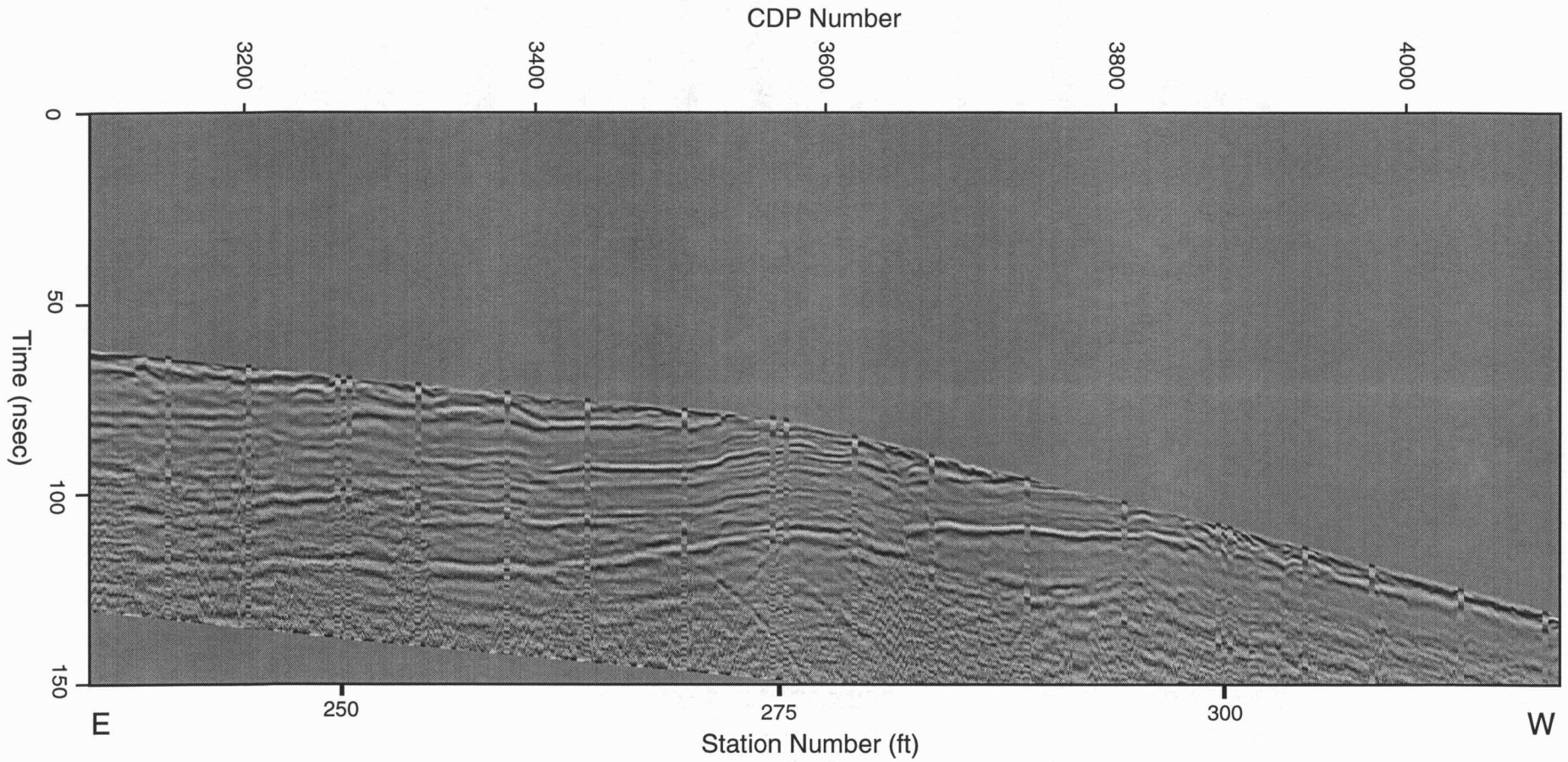

Figure 6b (Uninterpreted). The western portion of the GPR profile.